PASJ: Publ. Astron. Soc. Japan , 1–**??**,

Eruptions of Magnetic Ropes in Two Homologous Solar Events of 2002 June 1 and 2: a Key to Understanding an Enigmatic Flare

Nataliya S. Meshalkina[1,2], Arkadiy M. Uralov[2], Victor V. Grechnev[2], Alexander T. Altyntsev[2], and Larisa K. Kashapova[2]

[1]*Nobeyama Radio Observatory, Minamimaki, Minamisaku, Nagano 384-1305*
mtssnami@yandex.ru
[2]*Institute of Solar-Terrestrial Physics, Lermontov St. 126A, Irkutsk 664033, Russia*

(Received ???; accepted ???)

Abstract

The goal of this paper is to understand the drivers, configurations, and scenarios of two similar eruptive events, which occurred in the same solar active region 9973 on 2002 June 1 and 2. The June 2 event was previously studied by Sui, Holman, and Dennis (2006, 2008), who concluded that it was challenging for popular flare models. Using multi-spectral data, we analyze a combination of the two events. Each of the events exhibited an evolving cusp-like feature. We have revealed that these apparent "cusps" were most likely mimicked by twisted magnetic flux ropes, but unlikely to be related to the inverted Y-like magnetic configuration in the standard flare model. The ropes originated inside a funnel-like magnetic domain whose base was bounded by an EUV ring structure, and the top was associated with a coronal null point. The ropes appear to be the major drivers for the events, but their rise was not triggered by reconnection in the coronal null point. We propose a scenario and a three-dimensional scheme for these events in which the filament eruptions and flares were caused by interaction of the ropes.

Online material: mpeg animations.

Key words: Sun: filaments — Sun: flares — Sun: radio radiation — Sun: UV radiation

1. Introduction

Close association between eruptive phenomena and flares is well known, but causal relations between them have not yet been well understood. Several models have been proposed to describe the vast variety of phenomena observed in flares and eruptions. However, observations sometimes offer challenges for the existing models. In particular, coronal magnetic configurations in some events remain unknown.

For example, many properties of long-decay eruptive flares appear to be described by the "standard" flare model sometimes also referred to as "CSHKP" for its main contributors (Carmichael 1964; Sturrock 1966; Hirayama 1974; Kopp & Pneuman 1976). This model was advanced in many later studies, e.g., Somov (1992; 2006); Shibata et al. (1995a; 1995b; 1996; 1999); Yokoyama & Shibata (1998; 2001), etc. In this scenario, the major energy release occurs in magnetic reconnection in a vertical current sheet after an eruption of a magnetic filament, rope, or plasmoid. A range of probable causes of the appearance and acceleration of the ejection has been considered, from the emergence of a twisted magnetic flux rope from below the photosphere up to a gradual breakout reconnection high in the corona. The ejected plasmoid, in turn, eventually evolves into a coronal mass ejection or its part. One of the attributes of this model is the cusp region at the bottom of the current sheet. Shrinking flare loops are considered to be formed in the cusp region. Attempts to relate the standard model to observations of flares sometimes stumble upon problems, especially when impulsive flares are considered. For example, cusps occasionally appear in impulsive flares, but too late, when the major plasma heating and particle acceleration processes are almost completed (see, e.g., Grechnev & Nakajima 2002; Grechnev et al. 2006a; Sui et al. 2008).

An intriguing impulsive eruptive flare which occurred on 2002 June 2 was presented by Sui et al. (2006; 2008). The authors discovered several puzzling facts in the morphology and sequence of events observed in this flare. Multiple-loop interactions appeared to be the cause of the flare. The authors considered the emerging flux model (Heyvaerts et al. 1977) and the magnetic breakout model (Antiochos et al. 1999) and found both of them to explain some changes of the loop morphology in the flare; however, none of these models was found to explain all observational facts. Sui et al. (2006) characterized the situation as an "enigma of a flare involving multiple-loop interactions". The enigma consisted of the following problems. Some erupting features resembled magnetic flux ropes, but their nature and role in the events were unclear. One more problem was related to an apparent dynamic formation of a cusp-like feature observed in the event after the termination of the impulsive phase of the flare. The nature of the "cusp" remained unclear. The standard model did not seem to explain the phenomena, but the data that Sui et al. (2006; 2008) employed were not decisive in choosing an alternative model.

To address these unresolved issues, we note that another, very similar eruptive event occurred in the same

active region (AR) 32 hours earlier, on June 1. Both the June 1 and 2 events exhibited much the same manifestations: very short durations of ≈ 10 minutes in soft X-rays (SXR), comparable durations and total fluxes of hard X-ray (HXR) and microwave bursts, analogous eruptions and cusp-like features observed in extreme ultraviolet (EUV), and similar flare configurations of a comparable size seen in EUV, SXR, and HXR.

Various data are available for the June 1 event, i.e., 195 Å images from the Transition Region and Coronal Explorer (TRACE, Handy et al. 1999), microwave images from the Nobeyama Radioheliograph (NoRH, Nakajima et al. 1994), magnetograms from the Michelson Doppler Imager (MDI, Scherrer et al. 1995) and EUV images from the Extreme-Ultraviolet Imaging Telescope (EIT, Delaboudinière et al. 1995) on SOHO, as well as X-ray data from the Reuven Ramaty High-Energy Solar Spectroscopic Imager (RHESSI, Lin et al. 2002). Utilizing this comprehensive data set for the June 1 event and using the striking similarity between the June 1 and 2 events, we endeavor to understand their "enigma". Our advantages as compared to the study of Sui et al. (2006; 2008) are the possibility to combine findings from observations of both these events and the availability of NoRH microwave images for the June 1 event.

The goal of our study is to reveal the scenario of the two homologous June 1 and 2 events, their magnetic configurations, and major drivers. Section 2 addresses the observations. Section 3 summarizes the observational results and outlines a combined scenario of these eruptive events. Section 4 summarizes our findings and conclusions.

2. Observations and Analysis

2.1. Summary of both events

Two similar impulsive eruptive events occurred in AR 9973 ($\beta\gamma$-configuration) on 2002 June 1 and 2 (figure 1). The first event was associated with an M1.5 flare (S19 E29) on June 1, which started at 03:50 (all times hereafter are UT), peaked at 03:57, and ended at 04:01 according to GOES reports. The second event was associated with a C9.4 flare (S20 E09) on June 2 (11:41–11:47–11:50). Figure 1 shows some representative data related to both events (June 1 left, June 2 right). The scales are the same for both events.

Total duration of each event was $\approx$10 min. Both events contained impulsive parts of $\sim$2 min followed by longer thermal tails in low-energy RHESSI bands < 25 keV. The impulsive parts had comparable fluxes in X-rays and microwaves, while HXR and radio fluxes were somewhat weaker in the June 2 event. The June 1 event contained the second enhancement from 03:55:30 to 03:59, which was rather weak in HXR at > 25 keV, but strong in microwaves. The corresponding second enhancement was weak in the June 2 event.

We estimated the temperature and emission measure from two SXR bands of GOES-10 following White et al. (2005). In both events, the average temperature reached about 15 MK at the main peak. For the June 1 event, the total emission measure was 2×10^{48} cm^{-3} at the impulsive peak (03:54). With a size of the SXR-emitting region of about 7 Mm (from a RHESSI 3–6 keV image), the plasma density was 7×10^{10} cm^{-3} at that time. The thermal microwave flux estimated for the June 1 event was ≤ 7 sfu. Similar parameters were estimated for the June 2 event. They suggest that the microwave bursts were almost entirely non-thermal.

TRACE observed both events in the 195 Å band with an interval of 17 s. There were gaps in observations of the second event during 11:45:44–11:55:06. The TRACE 195 Å images in figures 1f and 1h show the pre-flare configurations to be similar (S-like) in shape, and figures 1g and 1i show basically similar eruptions of mutually wrapped structures. We produced TRACE 195 Å movies of either events TRACE_195_2002_June_01.mpg and TRACE_195_2002_June_02.mpg, having nonlinearly processed the images to reveal features of interest. The movies also show a great deal of similarity between the two events.

Filaments existed in the active region before either event. In both cases, S-like structures (marked "S" in figures 1f and 1h) resembling flare ribbons brightened up, and then their eastern parts rose and erupted. Later on, their remainder parts and the central regions became the footpoint areas of the flare loops. During the events, stripes appeared adjoining the S-like structures from the south and southeast as their extensions (figures 1g and 1i). All visible phenomena on the solar surface were confined by the outermost boundary of the S-like structure, the stripes, and footpoint areas of the flare loops. We call this boundary a *ring structure* (see double contour in figure 4e). This boundary suggests that a nearly closed magnetic structure confined the volume of the event. The cusp-like features as well as erupting dark filaments and bright ropes were visible in both events. The erupting filaments and ropes mutually wrapped, pushed their way through the coronal configuration which confined them, and escaped as a broad jet followed by outflowing dark material (surge). The impulsive flares occurred at the same time. Using the similarity between the two events, we combine findings from observations of each events.

2.2. The June 1 Event

2.2.1. The Configuration of the Flare Region

The event of June 1 was imaged by the NoRH at 17 GHz (both Stokes I and V). During the flare, the NoRH beam size was $13.3'' \times 12.8''$. Microwave images obtained during flares usually show a simple picture consisting of a few major sources in which strong gyrosynchrotron emission predominates. Nevertheless, microwave data carry information about features which could be weaker, especially prior to the main flaring, but important for understanding this complex eruptive event. Figure 2 shows a TRACE 195 Å image (a) and a SOHO/MDI magnetogram (b) as well as white-light image (c) with superimposed contours of microwave sources. The TRACE image in figure 2a shows the ring structure consisting of the S-like configuration and two southern stripes (indicated in figure 1g)

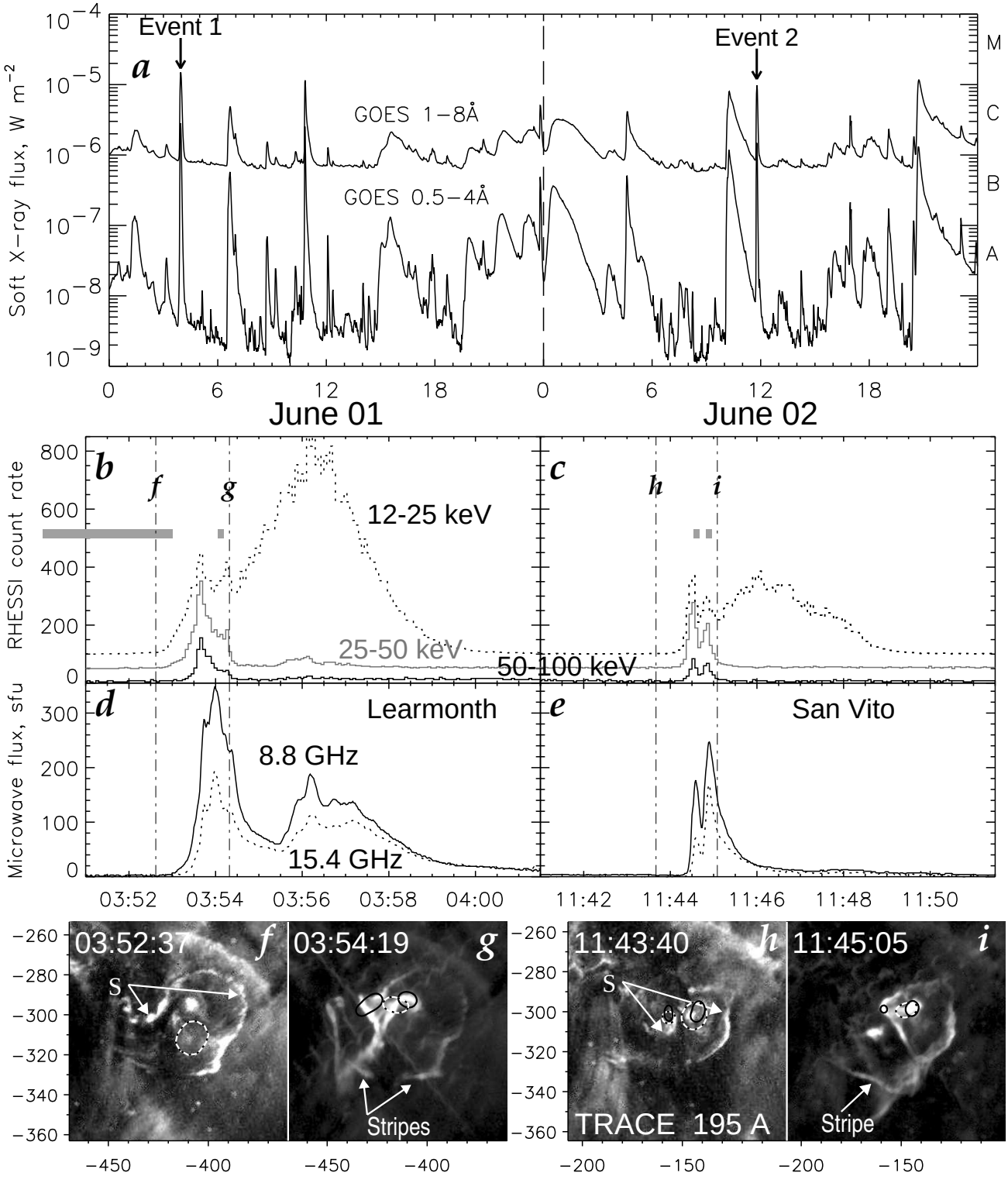

Fig. 1. Summary of June 1 and 2 events. GOES SXR flux (a), RHESSI count rates (b,c; vertically shifted for a better view), microwave total flux (d,e), and TRACE 195 Å images (hereafter, the axes show the distance in arcsec from the solar disk center) just before (f,h) and during the eruptions (g,i). Vertical broken lines (b–e) mark the central times of the TRACE images. Contours (f–i) are RHESSI images constructed with the Pixon method at 6–12 keV (dotted; 3–12 keV in panel f) and 25–50 keV (black) over intervals shown in panels b and c by gray bars. Contour levels are 40% of the maximum brightness for event 1 and 30% for event 2. All images hereafter are shown nonlinearly to reveal the features of interest.

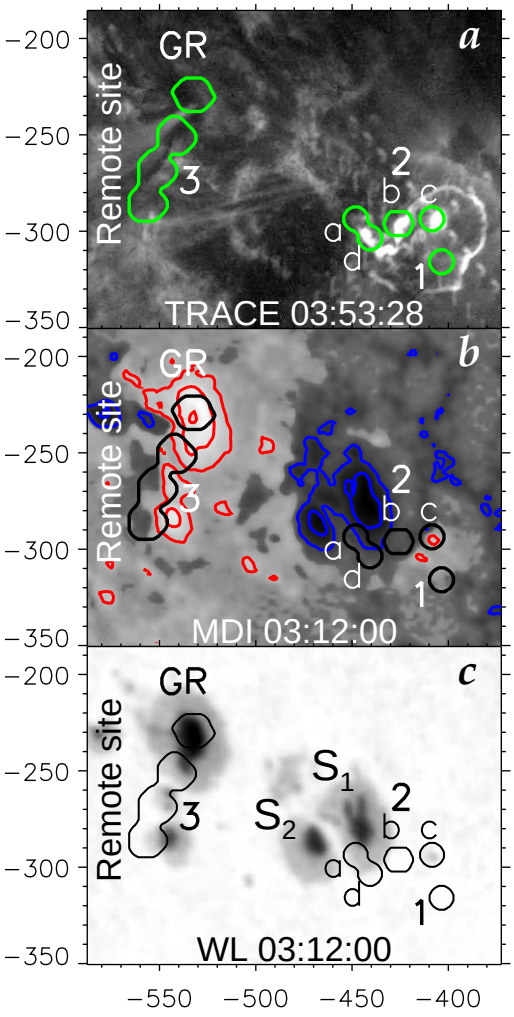

Fig. 2. The June 1 event. Contours of 17 GHz flare sources 1–3 (green and black) superimposed on a TRACE 195 Å image (a), an MDI magnetogram (b), and an MDI white–light image (c). Light areas and red contours represent N-polarity, dark areas and blue contours show S-polarity (levels $\pm 500\,\mathrm{G}, \pm 1500\,\mathrm{G}$).

before and during the flare.

Two microwave-emitting regions labeled 1 and 2 were located within the main flare site (see figure 3d), while it is possible to discern four components a–d of region 2. Component 2a was in between the S-polarity sunspots S_1 and S_2 (figure 2). Component 2c was located at a small N-polarity sunspot. A 70%-polarized steady gyroresonance source labeled "GR" coincided with a large N-polarity sunspot. A remote elongated region 3 was located south of it.

2.2.2. TRACE 195 Å and 17 GHz data

Figure 3 shows the pre-flare situation, and figure 4 presents some milestones of the entire event. The S-like structure appeared in 195 Å images at 03:20:27 (figures 3 and 4; earlier images are not shown). The eastern part of the S-like structure erupted during the event. The behavior of this feature suggested that it was a magnetic flux rope (denoted B_1 in figure 4b). A dark filament was visible south of rope B_1. Some of the long, dark filament barbs occulted the bright rope B_1 (figures 4c and 4d); hence, the rope must be located under the filament.

At about 03:47, the western part of the S-structure brightened and then started to expand outwards like a flare ribbon. Rope B_1 started to move southwards under the filament. The eruption occurred at 03:53–03:55 (figures 4e–h); rope B_1 brightened, stretched, bent, carrying the dark filament away, and finally disrupted. This interval corresponded to the first microwave peak (see figure 5). Dark outflow was afterwards seen in 195 Å and Hα images as a surge.

We have revealed active flare sources at 17 GHz by analyzing the variability of microwave images (Grechnev 2003; Grechnev et al. 2006c). The time profiles of the average brightness temperature in total intensity and polarized emission for each source are shown in figure 5.

In microwaves, region 1 brightened before the flare (figures 2 and 5). Its gradual time profile suggests its mainly thermal nature. Components a–d of region 2 were almost merged in total intensity, but distinct in polarized emission. Region 2a made a smaller contribution to the second peak than did regions 2b–d (the main Stokes I source slightly shifted southwards during the second peak). The similarity of the time profiles of sources 2a–d in the main flare site (figure 3d) and the remote source 3 indicates a connection between them during the first peak. Their connection is additionally supported by the anticorrelation of subsidiary peaks on top of the first main peak in the time profiles of regions 2c and 3 (see insets in figure 5). The absence of manifestations of the second main peak in region 3 suggests disconnection of regions 2 and 3 in the course of the event (cf. Kundu et al. 2001; Grechnev et al. 2003). A high degree of polarization observed in these regions supports their non-thermal nature.

2.2.3. Large-Scale Coronal Disturbances

Figure 6 shows coronal disturbances visible in a difference image composed by subtracting SOHO/EIT 195 Å images (03:58:33 and 04:05:33), both reprojected to 03:53:33 (close to the flare peak). The difference image shows an off-limb "EIT wave" and dimmings. The "EIT wave" was most likely due to a coronal shock excited by the eruption (see Grechnev et al. 2008). Neither the "EIT wave" nor dimmings were detected in NoRH images. The dimmings were located at the main flare site as well as the remote site highlighted by the microwave source 3, and also traced long loops between these sites. These loops were visible in TRACE and EIT images before the eruption and disappeared afterwards.

This fact confirms that their eruption and, together with a probable disconnection between the radio source 2c and the former source 3, suggests a change in the magnetic connectivity between the main and the remote sites.

Our TRACE_195_2002_June_01.mpg movie shows the following phenomena during the microwave second main peak (03:55:30–03:58:20): (i) the mutually twisted erupting structures transformed into a broad jet escaping from a confining coronal magnetic configuration; (ii) a wave-like disturbance propagated along the ring structure counter-

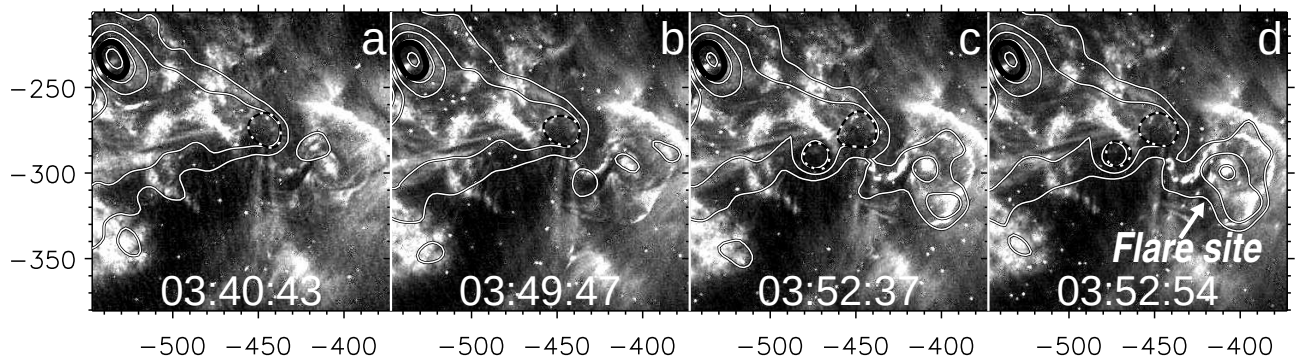

Fig. 3. TRACE 195 Å and 17 GHz images of the June 1 event over the pre-flare phase. The white solid contours (levels of $[12.5, 25, 50, 100, 200] \times 10^3$ K) show the total intensity. The black (in the upper left corner) and dotted contours show the positive and negative polarization respectively (50% of the maximum of the absolute value). Imaging intervals for both TRACE and NoRH are 10 s around the specified times.

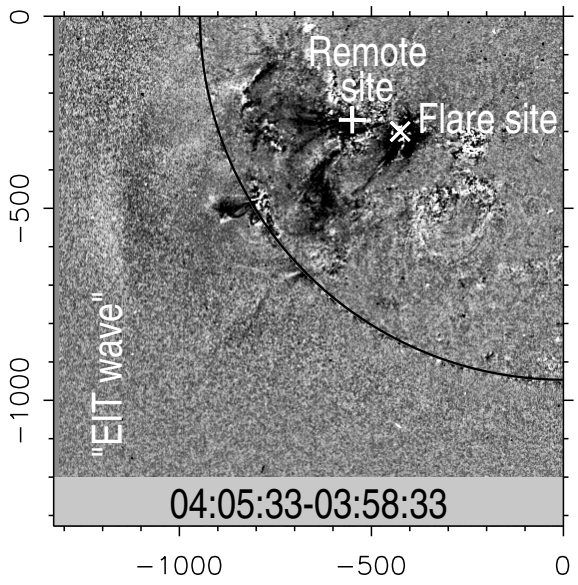

Fig. 6. "EIT wave" and dimmings in a SOHO/EIT 195 Å difference image of the June 1 event.

clockwise, and (iii) weak threadlike brightenings flickered near the remote site concurrently with the wave-like disturbance as its counterpart. All these phenomena suggest a possible reconnection between the escaping ejection and the surrounding magnetic field (see Section 3.3).

2.3. The June 2 Event

The overall story of the June 2 event previously addressed by Sui et al. (2006; 2008) was basically similar to the June 1 event. Some of its images observed with TRACE at 195 Å are shown in figure 7, and a movie is available in the electronic version of this paper. We processed these images heavier than did Sui et al. (2006), which allowed us to reveal important features.

A bright twisted rising feature visible in figures 7a and 7b, which we call rope A, was filled with material probably at a coronal temperature. It appeared well before the event and disappeared after 11:35. Most likely, the rope heated up (its temperature left the sensitivity range of the 195 Å channel) and erupted. A ring structure came into view later on.

The event started at about 11:44 with a brightening of the S-like structure (like the June 1 event). Its eastern part (rope B_1) expanded southwest (figures 7c–f). The western part moved west, and an erupting feature (presumably, yet another rope, which we call rope C) showed up in its structure (figures 7e–i). We did not see an analogous feature in the previous event. Figures 7g–i and a movie TRACE_195_2002_June_02.mpg display a collision of ropes B_1 and C to produce a combined ejection transforming into a broad outflowing jet. Rope B_1 turned southeast after the collision, i.e., by about 90° (figures 7f and 7g), as if its expansion were confined by a funnel.

The TRACE images were distorted due to interference on the CCD detector, so that it is difficult to distinguish real features from the interference fringe. Nevertheless, signatures of untwisting ropes are detectable. Dark outflowing material (a surge) is also visible in figures 7g–l.

2.4. Evolution of Active Region 9973

Similarity between the June 1 and 2 events implies the persistence of the main photospheric configuration and reproduction of pre-event conditions. Figure 8 presents the evolution of AR 9973 shown by MDI magnetograms (see also the movie MDI.mpg). Figures 8a and 8b, and 8d and 8e show the magnetograms. Figures 8c and 8f show the negatives of variance maps computed from the magnetograms over intervals including the events (specified in the panels). Each variance map (Grechnev 2003) was formed by calculating the variance for each pixel in a set of magnetograms along their temporal dimension. The most variable regions are seen in figures 8c and 8f as the darkest patches. The major changes were the development of sunspot S_1, the diminishing of the N-polarity area (black contour in figure 8b) inside the ring structure (white dotted contour), and motions of magnetic elements near the boundary of a supergranular cell.

The development of sunspot S_1 was manifest in increased field strength in its southwestern part and a later

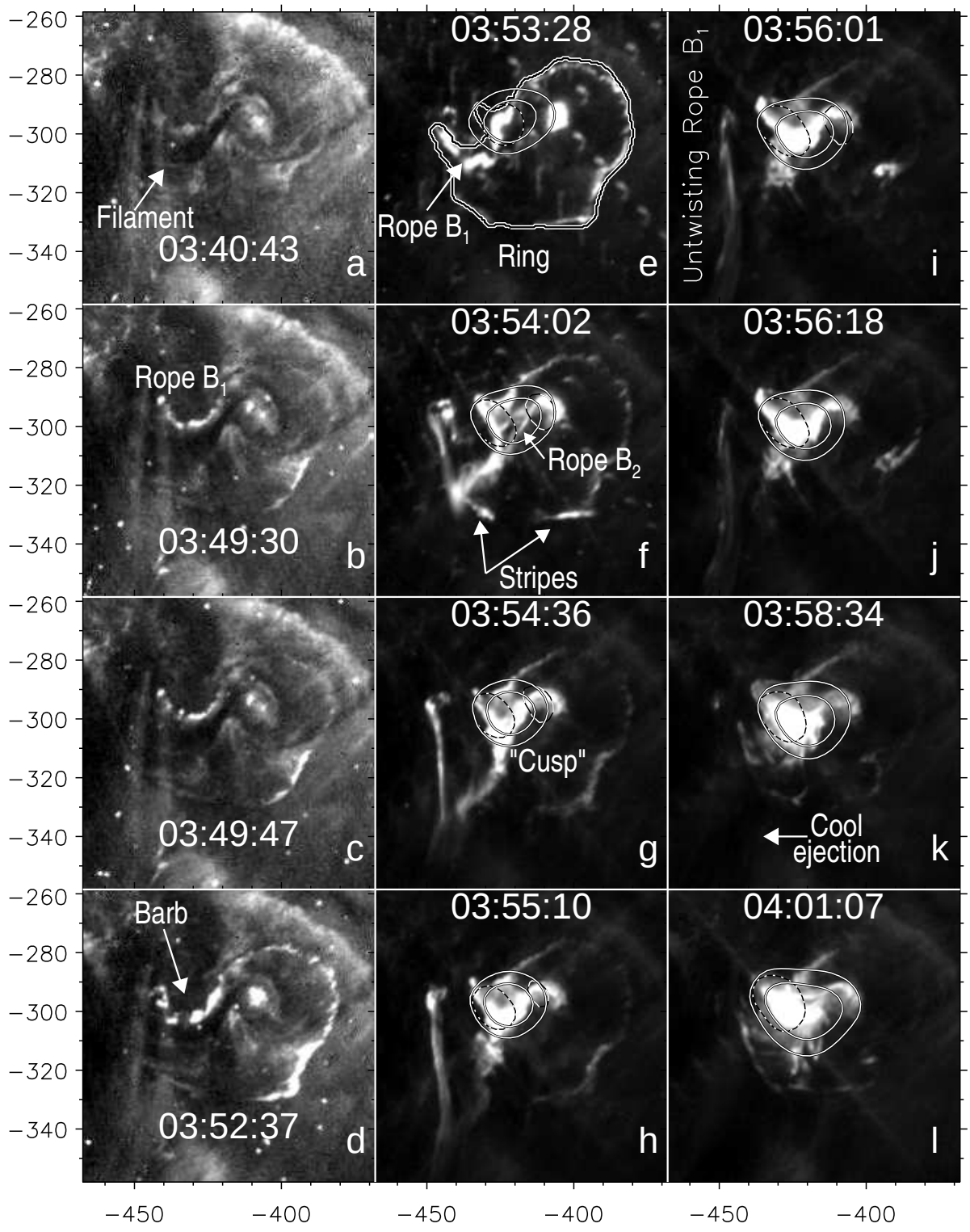

Fig. 4. TRACE 195 Å and simultaneous 17 GHz images of the June 1 event. The white solid contours show 20% and 50% of the maximum intensity. The broken contours show the polarization (Stokes V, dotted negative, dashed positive, both 50%). Contours of the 17 GHz images in the previous figure are not shown in the left column. The double contour in panel (e) shows the outer boundary of the ring structure. Slanted cross-like dark/bright patterns in TRACE images are due to interference from bright features on the CCD detector.

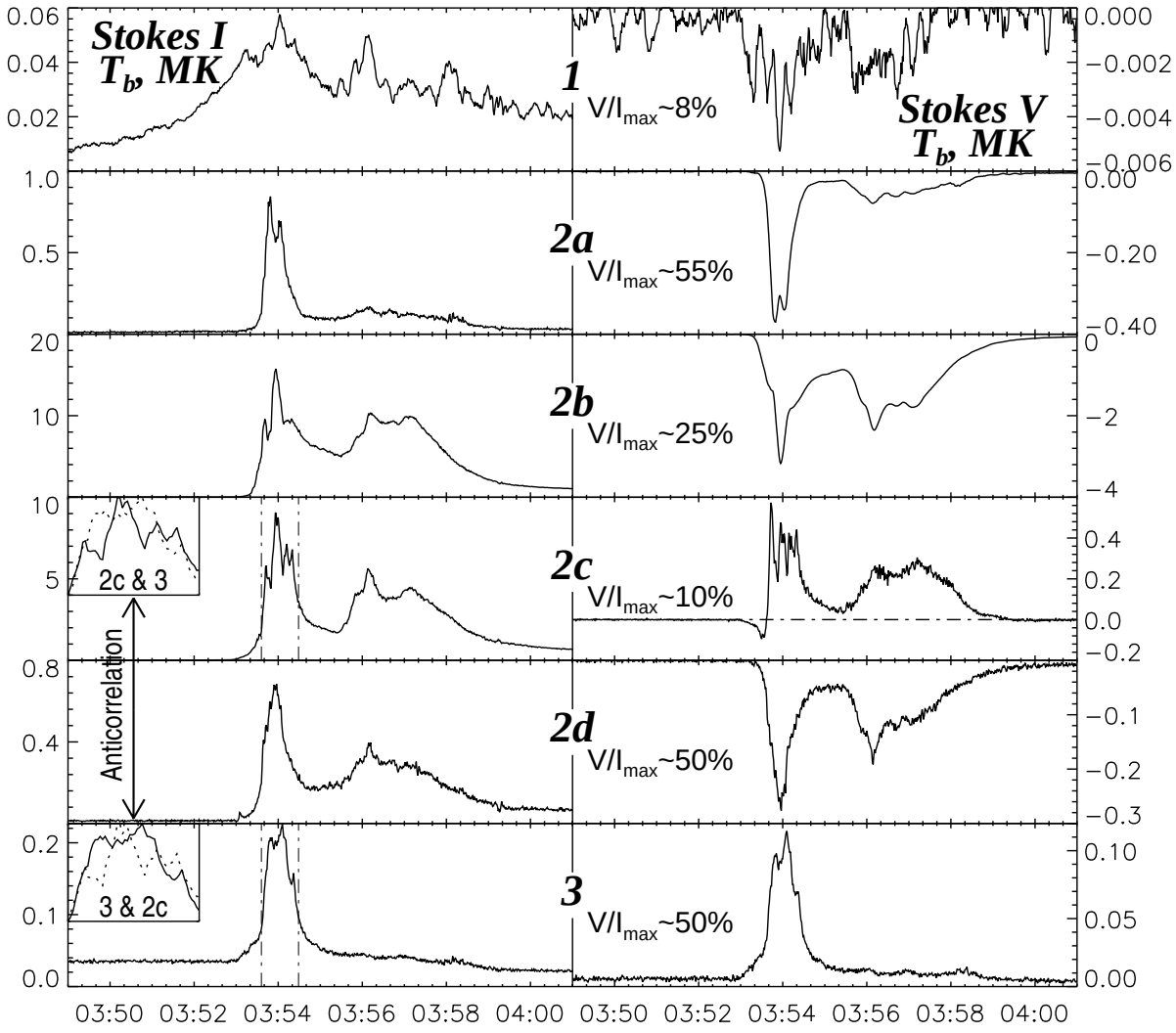

Fig. 5. The June 1 event. Time profiles of the average brightness temperature at 17 GHz in total intensity (left) and polarization (right). "V/I$_{max}$" is the maximum degree of polarization in each region.

growth of a narrow extension which stressed the eastern part of the S-like structure (figure 8e). The small N-polarity area diminished and eventually disappeared on June 3. The environment of the S-structure (the boundary of the supergranular cell) exhibited variations, while the western part of the S-structure was within a relatively quiet area and remained almost unchanged. Thus, the evolution of the active region explains the homology of the June 1 and 2 events and their differences.

3. Summary and Interpretation

Using the resemblance of the June 1 and June 2 events, we combine all observational findings in both these events, as if they were a single event.

3.1. Outline of the Coronal Magnetic Configuration

The main magnetic flux of AR 9973 was confined within a bipolar structure consisting of an eastern N-polarity area and a western S-polarity area (see figure 2b). The photospheric region of the volume in which the eruptive events occurred was encompassed by the ring structure (the white dotted contour in figure 8b), suggesting its correspondence to the separatrix base (the dashed semi–oval in figure 9 and the dashed circle in figure 10). The ring structure was located inside the extensive western S-polarity area and encompassed an N-polarity island (black contour in figure 8b). The total fluxes of the N- and S-polarity magnetic fields calculated inside the ring structure separately for the June 1 event were approximately equal to each other (imbalance $<10\%$). This fact favors an assumption that the magnetic flux of the N-polarity island was mainly closed within the volume where the events occurred. An additional support to this assumption is provided by the fact that all observed motions of the erupting features in either event were confined within a "funnel".

The ring structure looked like a flare ribbon occulted by a multitude of dark absorbing features crossing it (see

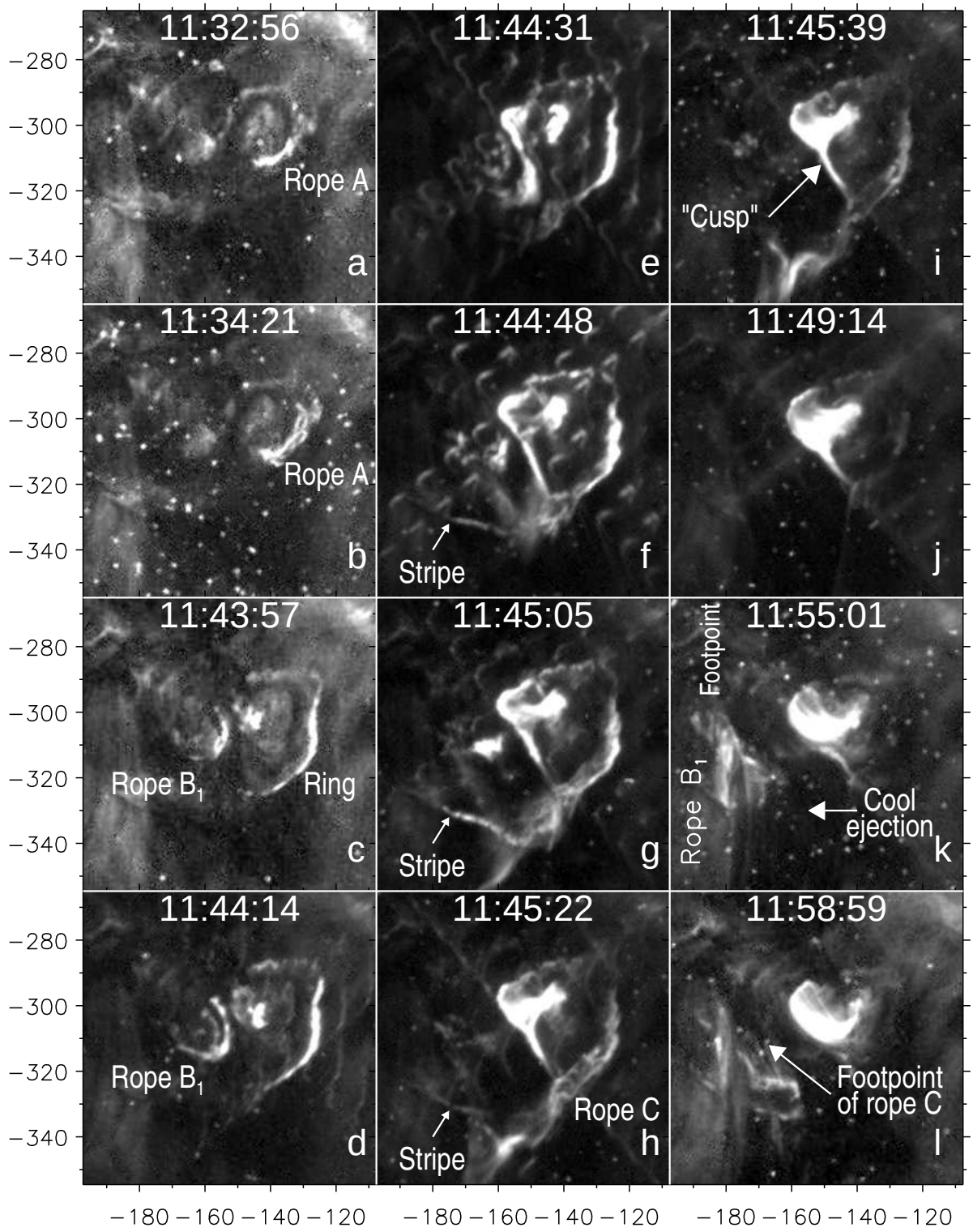

Fig. 7. TRACE 195 Å images of the June 2 event.

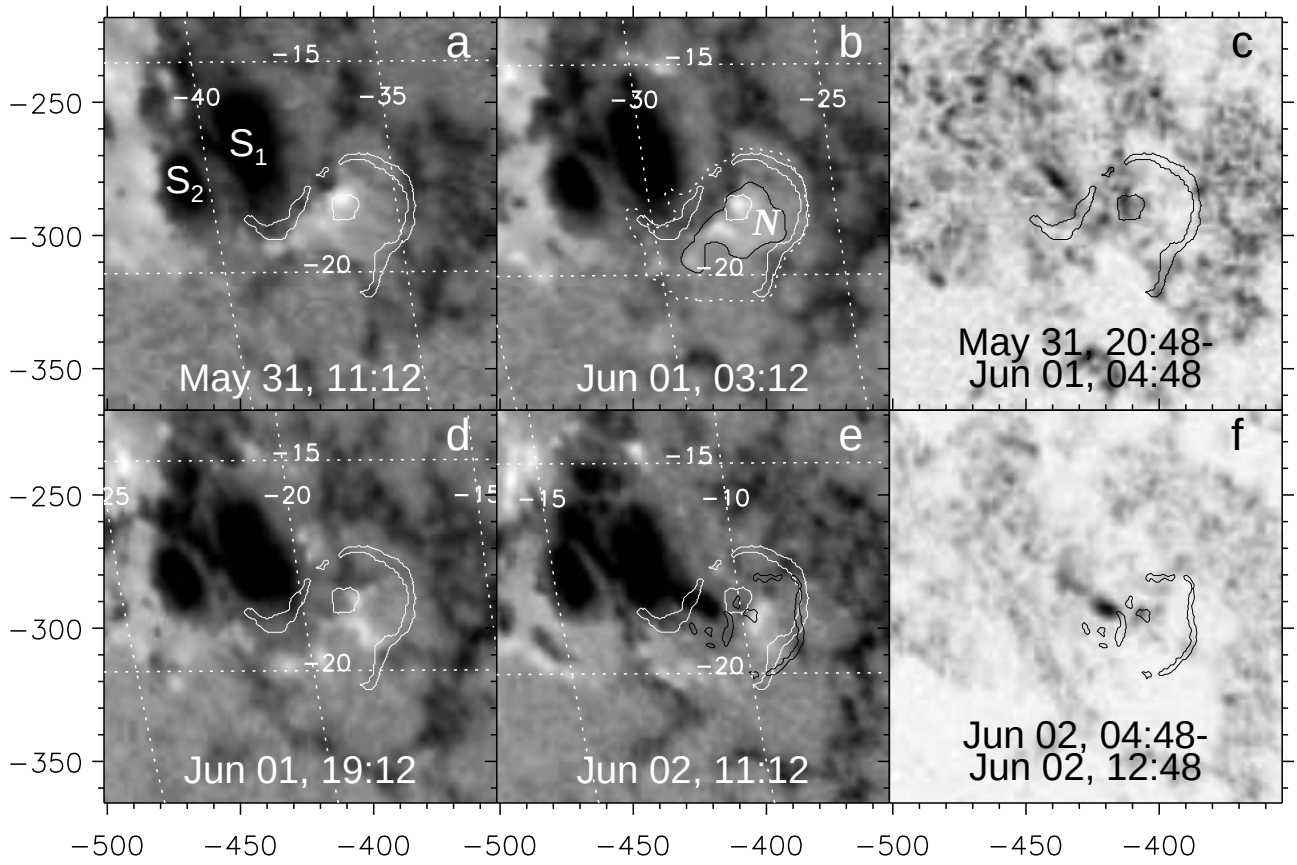

Fig. 8. Evolution of AR 9973. Panels a,b, and d,e show SOHO/MDI magnetograms; panels c,f show the negatives of variance maps produced from the magnetograms over specified intervals. The S-like structure visible in TRACE 195 Å images is shown by the white solid contours for June 1 (black in panel c) and black contours for June 2 (in panels e, f). The white dotted contour in panel b shows the ring structure, and the black contour in this panel delineates the N-polarity island. All the images are re-projected to the June 1 event. The white dotted grid (a–e) shows the actual heliographic coordinates for each image.

the western part of the ring structure in figures 4c–h and its southern part in figure 7g labeled "Stripe"). We are aware of a single paper describing a similar phenomenon (Borovik & Myachin 2002). Some parts of the ring structure resembled a quasi-stationary "EIT wave" stopping at the separatrix surface. Such an "EIT wave" might be due to a successive stretching of closed field lines (e.g., Chen et al. 2005) driven by erupting flux ropes. The concept of a separatrix surface is an idealization; instead, a quasi-separatrix layer (Démoulin et al. 1996) appears to match a realistic situation better. The intersection of such a layer with the base of the corona should be a set of stripes, which resembles the appearance of the ring structure.

Our considerations lead to a configuration of the equilibrium coronal magnetic field shown in figure 9 with a coronal null point at its top (cf. Filippov 1999; Gary & Moore 2004). The presence of a null point implies a possibility of magnetic reconnection high in the corona. A subsequent analysis, however, does *NOT* show the role of magnetic reconnection in the coronal null point to be a crucial factor in the initiation of the June 1 and 2 eruptive events.

3.2. Magnetic Flux Ropes

According to Lites (2005), the presence of magnetic flux ropes "may be rather common in normal (i.e., non-δ-type) active regions", and several flux ropes appeared to be involved in the events. We call them ropes A, B, and C according to their sequence in the "combined event" of June 1 and June 2. Figure 9 outlines the pre-flare positions of ropes A and B as well as the filament inside the volume enclosed by the separatrix surface. The outer edge of the red/blue semi-oval shows its intersection with the photosphere. Figure 10 shows the projection visible from above (without the filament). The twist in the eastern footpoint of rope B_1 visible in figure 7k means that the electric current and the magnetic field are parallel. The same direction of twist is assumed for ropes A and C.

Rope A appeared (see figures 7a and 7b) 8 min before the onset of the SXR flare (GOES). The position of its visible southern footpoint corresponded to the N-polarity. After its eruption, the ring structure (figures 7c and later frames) appeared simultaneously with the onset of the event in SXR. A probable nature of the ring structure was discussed in Section 3.1.

Rope B could appear (and start to move afterwards) in

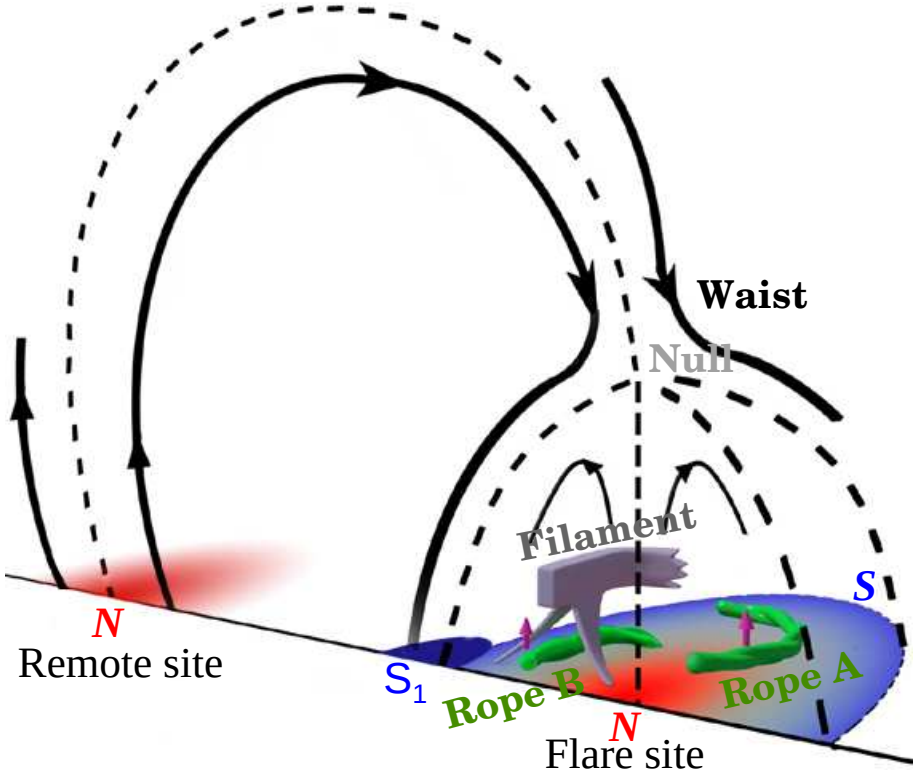

Fig. 9. The situation before the June 1 and 2 flares. The N-polarity is red, the S-polarity is blue, the neutral area is gray). Dashed lines denote separatrices, the separatrix surface and its intersection with the photosphere. A coronal null point is at the top of the volume in which the events occurred. The remote site corresponds to the microwave source 3. The frontal surface of the figure corresponds to a cross section denoted by the arrows in figure 10. Rope A rose and disappeared first. Next, rope B started to rise below the filament (gray), which remained motionless.

the course of evolution of a low magnetic structure due to photospheric motions and magnetic reconnection. The brightening of the rope before its eruption could also be due to reconnection. To co-ordinate our discussion with observations, we consider rope B to consist of two interconnected ropes B_1 and B_2 (figures 9,10 and 4,7). In the June 1 event, rope B_1 appeared under a dark filament like a bright ribbon visible between barbs. This rope showed a large twist of magnetic fields lines near its eastern footpoint F_{B1S} (figures 11, 4i and 4j, 7k and 7l, and movies). As the rope stretched, the twist decreased. Rope B_2 manifested itself during the flare (figures 4f and 4j).

One cannot rule out a possible emergence of ropes B_1 and B_2 from below the photosphere. Another possibility to propel rope B_1 was an extra twisting of its eastern footpoint F_{B1S}. Photospheric horizontal flows seen in the periphery of sunspots S1 and S2 appear to collide near this footpoint (see the attached MDI movie). The history of rope B_2 is uncertain. Its presence was indicated by the cusp-like features and suggested by the location of the main flare site in both events being separated from a slow magnetic reconnection between ropes B_1 and B_2 probably started before the flare. Later, the ropes entered the fast flare reconnection stage and was combined into an interacting loop system which we call rope B.

Rope C (figure 7h) roughly corresponds to the blue rope in figure 7 (lower middle panel) of Sui et al. (2006). A possible position of its eastern footpoint is shown in figure 7l. Rotating motion of the rope was visible, but its direction here remains unclear.

We assume the magnetic configuration consisting of flux ropes and overlying magnetic field confining them to be metastable (see, e.g., Sturrock et al. 2001, Rachmeler et al. 2009), and the toroidal forces (Shafranov 1966, Chen 1989, Garren & Chen 1994) in rope B_1 to be the major driver of the eruption. A system is metastable if it is stable (due to confining fields) against small perturbations, but unstable to sufficiently large perturbations (e.g., displacement, additional twist, or plasma pressure increase). Therefore, an impulsive release of magnetic energy is possible in such a situation. This can lead to the ejection of the rope. If the amount of twist in it was sufficiently large, the rope was able to protrude like a hernia through the confining magnetic field and escape, while the overlying field lines slid, without breaking, towards the anchored ends of the rope. The assumption that the twist of rope B_1 was really large is supported by the inclination angle of field lines in its eastern leg (figure 7k) which shows that the poloidal component of the magnetic field B_p was nearly equal to the toroidal component B_t there. With the observed ratio of the length to radius of rope B_1 being $L/r \geq 5\pi$ (see figures 4b and 4c and 7d), the equality

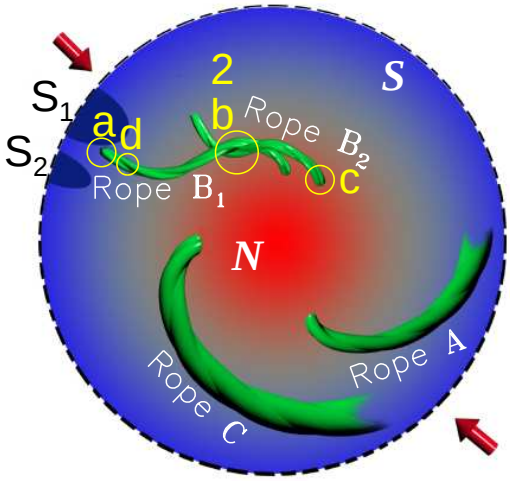

Fig. 10. Top view of figure 9: probable positions of magnetic flux ropes (green). The area is bounded by the intersection of the separatrix surface with the photosphere (the outer dashed circle). The background shows the magnetic polarity at the photosphere. Ropes B_1 and B_2 are components of rope B. The dark filament above is not shown. Open ends of ropes A and C indicate that the positions of their footpoints are not known. All the ropes are probably inter-related. Yellow circles denote microwave flare sources.

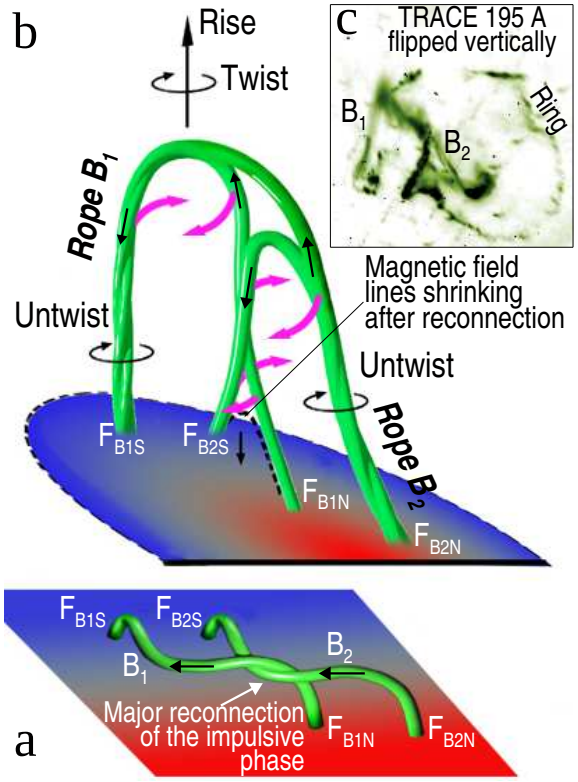

Fig. 11. Partial magnetic reconnection of ropes B_1 and B_2, their joint rise, and rotation. The black arrows on the ropes indicate the directions of electric currents. a) The initial position of the ropes. b) The situation after the impulsive phase. c) A negative of the TRACE 195 Å image at 03:54:02 flipped vertically to match the scheme.

of B_t and B_p gives the amount of twist in rope B_1 to be $L/(2\pi r)B_p/B_t \geq 2.5$. Such a total twist provides sufficient energy to drive an eruption (see, e.g., Sturrock et al. 2001).

3.3. Flare, Ejecta, and a Cusp-like Feature

Figure 11 shows a scheme of the interaction between ropes B_1 and B_2. The overlying field lines which prevent the expansion of the configuration are not shown. The directions of the electric currents in the ropes are indicated by black arrows. Footpoints F_{B1S}/F_{B1N} of rope B_1 and F_{B2S}/F_{B2N} of rope B_2 are assumed to be fixed during the flare. The concept of mutual interaction of magnetic flux ropes and the rule of a helical kink of a current-carrying magnetic loop (e.g., Uralov 1990) were used in drawing this scheme. Figure 11a outlines the initial locations of the ropes in static condition.

Rope B_1 rose for 3 min under the static filament, and the observations did not show any motion of rope B_2 at that time. Once the magnetic reconnection between ropes B_1 and B_2 has started, their mutual configuration will determine the maximum rate of reconnection, because the parallel components of currents in the ropes attract each other. When rope B_1 moved upward on one side of the filament, cutting its barbs and destabilizing it, the first main peak of the June 1 flare occurred (between the situations shown in figures 11a and 11b). Note that the measured acceleration of rope B_1 was maximum at the rising stage of the impulsive phase.

Figure 11b shows the situation after the impulsive phase. The "Untwist" arrows show an untwisting of the rising ropes just above their footpoints. The untwisting of the eastern leg of rope B_1 is visible in the attached two movies. The reasons of the untwisting can be illustrated by considering a freely expanding rope with fixed footpoints. The first reason is the expansion of the rope itself by conserving both its poloidal and toroidal magnetic fluxes (i.e., a decrease of the longitudinal current in the rope). The poloidal magnetic component decreases, and the toroidal component remains nearly constant just above a footpoint. The ratio of these components decreases at this place which looks like untwisting. The second reason is a helical bending of the whole rope that is accompanied by the decrease of the winding of the field lines inside the rope (as occurs in a kink instability). The pink arrows in figure 11b indicate the directions of motion for different parts of ropes B_1 and B_2 in their helical bending. The pair of the rising ropes rotates (the "Twist" arrow). The interacting parts of the ropes above F_{B1N} and F_{B2S} tend to wrap around each other. The crossing point of the ropes mimics a cusp structure (figures 11b and 11c). If the interacting parts of ropes B_1 and B_2 were infinitely long, then the direction of their mutual twisting would correspond to the "Twist" arrow. However, the ropes stayed side-by-side in the cusp region. The dashed line in Figure 11b shows a field line (flare loop) shrinking

down from the crossing point.

The cusp-like features were observed in the TRACE 195 Å channel (figures 4f–h, 7g–j). It is sensitive to the FeXII (0.5–2 MK) and FeXXIV (11–26 MK) emissions (Handy et al. 1999). Since hot features are known to be fuzzy (e.g., Tousey et al. 1973, Sheeley et al. 2004), the fine thready structures of the "cusps" imply that they were at normal coronal temperatures of about 1.5 MK. Conversely, the cusp related to the reconnection site in the standard model should be hotter [> 3 MK; see, e.g., Yokoyama & Shibata (1998; 2001)], and therefore the appearance of the observed "cusps" does not match the expectation. Also, the SXR 3–12 keV source in figure 1f probably related to the coronal null point was observed on June 1 as early as 03:50–03:53, but the "cusp", which must be associated with the SXR source, was formed later (see figures 4e–g), being not co-spatial with it. Thus, the "cusps" most likely had no relation to the inverted Y-type configuration in the standard model, but were mimicked by cooler magnetic ropes.

Reconnection went on after the impulsive phase, because the magnetic fields at the top of the cusp-like structure became nearly antiparallel due to the stretch of the ropes. However, the reconnection rate declined because the electric currents in the ropes became also antiparallel and repelled each other. Both these factors resulted in intertwisting of the ropes (see also Hansen et al. 2004). Note that the dual-rope initiation of a flare (figure 11) resembles the scheme proposed by Uralov et al. (2002) and Grechnev et al. (2006d).

The dual-rope configuration in figure 11b was distorted due to its instability to a helical twist. Moreover, the distortion of ropes B and C was also influenced by the outer magnetic structure encompassing the volume in which the events occurred. This volume resembles a "funnel" with a narrow waist (see figure 9). The lower part of this "funnel" is bounded by a hemispheric separatrix surface. The optimal escape path of ejections runs through the waist. The "magnetic funnel" confines the ejections as suggested by the movies. The interaction of the ejections with this "funnel" and their pass through the waist appear to have produced a wave disturbance in the corona observed as an "EIT wave" (see Section 2.2.3) rapidly expanding above the limb.

The motion of the mutually wrapped dual-rope ejection through the waist must be accompanied by reconnection of the magnetic field lines of the ejection with those of, or near to, the separatrix surface. A response to this process could be concurrent EUV disturbances that propagate along the ring structure and near the remote site (see Section 2.2.3 and figure 9).

3.4. Microwave Emission in the June 1 Event

The microwave pre-flare emission was mainly thermal, as shown by contours in figure 3, and the only compact microwave sources were related to the major sunspots. The ring structure appeared in microwaves, too, similarly to EUV (see figures 3c and 3d), indicating heating. All flaring microwave sources (except for source 1) in figure 2 were non-thermal (see figure 5).

The flare sources 2a–d were located along rope B consisting of ropes B_1 and B_2 (figure 10). Source 2a was located in the eastern footpoint of rope B_1, where its untwisting was observed. Source 2b presumably corresponded to the intersection region of ropes B_1 and B_2. Source 2c was associated with the western footpoint of rope B_2. The time profiles in figure 5 suggest the connections between all of these flare sources. Their non-thermal nature and localization in ropes B_1 and B_2 indicate reconnection of the ropes, confirming the scheme in figure 11.

The detailed correspondence of the time profiles of the non-thermal sources 2 and 3 during the first main peak (see figure 2) suggests their connection. The long loops detected in the TRACE 195 Å images between sources 2 and 3 traced a magnetic channel connecting the flare and the remote sites. Particles responsible for the remote microwave source 3 could arrive from the main flare site through a change in magnetic connectivity while the ejection was passing through the waist (see Sections 2.2.3 and 3.3).

3.5. About Soft X-ray Sources

Sui et al. (2006, Section 2.3) have not revealed in the June 2 event any X-ray emission along the western part of the ring structure (which they called ribbon A). Similarly, no X-ray emission from this region was detected in the June 1 event. These facts confirm our conclusion that this feature was not a flare ribbon. Sui et al. (2006) also noticed in the same Section that the main SXR sources, as shown by RHESSI at 6–12 keV, corresponded to the footpoints in the June 2 event, which was unusual (see also our figure 1h). To explain this fact, Sui et al. (2006) suggested a low density and temperature in SXR-emitting loops, but our estimates (Section 2.1) do not confirm these assumptions. Another possibility could be an enhanced brightness of overlapping legs of the loops visible at small angles to the line of sight. The RHESSI SXR images in question temporally correspond to the TRACE 195 Å images in figures 7e and 7f, which clearly show structures with temperatures of 1–1.5 MK. Images of hotter (> 11 MK) structures coming at the same time in the FeXXIV passband of the TRACE 195 Å channel are expected to be darker and fuzzier than the 1–1.5 MK structures registered in its major FeXII passband (see, e.g., Tousey et al. 1973, Sheeley et al. 2004, Grechnev et al. 2006b). Hence, we would not be able to separate the hot and the cooler structures in the TRACE 195 Å images. However, the loops emitting at 6–12 keV are expected to appear at 195 Å after their cooling, and we simulated the SXR image from later TRACE 195 Å frames by blurring them to imitate their previous fuzziness. The result roughly resembles the RHESSI image in question and demonstrates that one might deal here with an effect of integration of the column emission measure explaining the enhanced SXR brightness of the footpoint regions.

3.6. Initiation of the Events and Flare Models

The geometry of the phenomenon inspires one to assume that the appearance of the ring structure and the eruptions were caused by magnetic reconnection in the coronal null point (see figure 9). In the breakout model, it is the first step initiating the eruption (Antiochos et al. 1999). However, observations in the present events did not show the role of the "breakout" reconnection high in the corona to be crucial in the triggering and course of the events for the following reasons.

1. The ring structure appeared after, rather than before, the eruption of rope A.
2. The outermost boundary of the ring structure was well-defined. Reconnection in a null point would not imply such a boundary.
3. The rise of rope B started under the almost static filament, which protected it from the influence of the "breakout" reconnection.

On the other hand, the rise and eruption of rope A preceded the onset of the event in SXR and EUV, and the eruption onset of rope B preceded the flare in microwaves and HXR. These facts indicate that reconnection in the lower corona (e.g., "tether cutting") was not a major launching factor for the events. This outcome is consistent with the conclusion of Sterling et al. (2001), "the tether cutting reconnection may still be occurring, but only after the eruption onset was triggered by some other process".

Unlike the standard model, in which flare reconnection is initiated by a rise of a single magnetic rope, we have discussed the initiation of the eruptive flares by reconnection of two rising ropes. This explains the location of the main flare site separated from the central, fastest-moving part of rope B_1. The dual-rope configuration mimicked the cusp, which had no relation to the hot cusp in the standard model. Reconnection between the ropes explains non-thermal radio emission from the eastern footpoint of rope B, the driver of the flare.

4. Conclusion

The combined multi-spectral analysis of two homologous eruptive events of 2002 June 1 and 2 allowed us to outline their common picture. Similarity of the photospheric conditions and persistent photospheric flows determined the resemblance between the events. The boundary of the sites where the events occurred was a time-evolving structure visible in EUV as a ring.

The observations left the impression that it was not possible to perceive the scenarios of the events by considering each of them separately. We have combined all the observed facts from both these events, as if they were a single event, and proposed their common scenario. We have concluded that their major drivers were eruptions of magnetic flux ropes. Neither the triggering of the events nor their evolution appear to be controlled by processes at the coronal null point. Such processes were probably present, but they did not determine the initiation of the events. The standard model, the breakout model, as well as other models employing magnetic reconnection high in the corona do not help to understand these impulsive events.

Sui et al. (2006; 2008) highlighted problems in the interpretation of the 2002 June 2 event in terms of widely accepted theoretical schemes and emphasized their importance. Interpretation of the two events made in our paper is based on a scheme involving the eruption of interacting flux ropes. The scheme is inherently three-dimensional and hardly reducible to the 2- or 2.5-dimensional geometry while maintaining its essence.

Acknowledgements. We thank K. Shibasaki, V.F. Melnikov, S.M. White, D.M. Prokof'ev and D.S. Meshalkin for fruitful discussions and assistance. We thank the referees for useful recommendations. We are especially indebted to the second referee for his attention and great efforts to improve the paper. The results presented here have become possible due to the usage of microwave imaging data obtained with the solar dedicated Nobeyama Radioheliograph operating continuously for over a decade. N.S.M., A.M.U., and V.V.G. wish to thank the staff of NRO/NAOJ (Japan) for their help and hospitality. This study was supported by the Russian project of RFBR No. 07-02-00101, 08-02-92204, 09-02-00226.

We are grateful to the instrumental teams of the NoRH, TRACE, RHESSI, and SOHO mission for their open-data policies. SOHO is a project of international cooperation between ESA and NASA.

References

Antiochos, S. K., DeVore, C. R., & Klimchuk, J. A. 1999, ApJ, 510, 485
Borovik, A. V., & Myachin, D. Yu. 2002, Sol. Phys., 205, 105
Carmichael, H. 1964, Proc. of AAS-NASA Symp. on the Physics of Solar Flares, W. N. Hess, NASA-SP 50, 451
Chen, J. 1989, ApJ, 338, 453
Chen, P. F., Fang, C., & Shibata, K. 2005, ApJ, 622, 1202
Delaboudinière, J.-P., Artzner, G. E., Brunaud, J. et al. 1995, Sol. Phys., 162, 291
Démoulin, P., Henoux, J. C., Priest, E. R., Mandrini, C. H. 1996, A&A, 308, 643
Filippov, B. P. 1999, Sol. Phys., 185, 297
Garren, D. A., & Chen, J. 1994, Phys. Plasmas, Vol. 1, No. 10, 3425
Gary, G. A., & Moore, R. L. 2004, ApJ, 611, 545
Grechnev, V. V., & Nakajima, H. 2002, ApJ, 566, 539
Grechnev, V. V. 2003, Sol. Phys., 213, 103
Grechnev, V. V., White, S. M., & Kundu, M. R. 2003, ApJ, 588, 1163
Grechnev, V. V., Kuzin, S. V., Urnov, A. M., et al. 2006a, Sol. Sys. Res., 40, 286
Grechnev, V. V., Uralov, A. M., Zandanov, V. G., et al. 2006b, PASJ, 58, 55
Grechnev, V. V., Kundu, M. R., & Nindos, A. 2006c, PASJ, 58, 47
Grechnev, V. V., Uralov, A. M., Zandanov, V. G. et al. 2006d, PASJ, 58, 69

Grechnev, V. V., Uralov, A. M., Slemzin, V. A. et al. 2008, Sol. Phys., 253, 263
Handy, B. N., Acton, L. W., Kankelborg, C. C. et al. 1999, Sol. Phys., 187, 229
Hansen, J. F., Tripathi, S. K. P., & Bellan, P. M. 2004, Phys. Plasmas, 11, 3177
Heyvaerts, J., Priest, E. R., & Rust, D. M. 1977, ApJ, 216, 123
Hirayama, T. 1974, Sol. Phys., 34, 323
Kopp, R. A., & Pneuman, G. W. 1976, Sol. Phys., 50, 85
Kundu, M. R., Grechnev, V. V., Garaimov, V. I., & White, S. M. 2001, ApJ, 563, 389
Lin, R. P., Dennis, B. R., Hurford, G. J. et al. 2002, Sol. Phys., 210, 3
Lites, B.W. 2005, ApJ, 622, 1275
Nakajima, H., et al. 1994, Proc. IEEE, 82, 705
Rachmeler, L. A., DeForest, C. E., & Kankelborg, C. C. 2009, ApJ, 693(2), 1431
Scherrer, P. H., Bogart, R. S., Bush, R. I. et al. 1995, Sol. Phys., 162, 129
Shafranov, V. D. 1966, in: M. A. Leontovich (Ed.), Revs. of Plasma Phys, Vol. 2, Consultants Bureau, New York, p. 103–151
Sheeley, N. R., Jr., Warren, H. P., & Wang, Y.-M. 2004, ApJ, 616, 1224
Shibata, K. 1995a, in Observational Plasma Astrophysics: Five Years of Yohkoh and Beyond, ed. T. Watanabe, T. Kosugi, & A. C. Sterling (Dordrecht: Kluwer), 187
Shibata, K., Masuda, S., Shimojo, M. et al. 1995b, ApJ, 451, L83
Shibata, K. 1996, in Magnetohydrodynamic Phenomena in the Solar Atmosphere: Prototypes of Stellar Magnetic, ed. Y. Uchida, T. Kosugi, & H. S. Hudson (Dordrecht: Kluwer), 13
Shibata, K. 1999, Ap&SS, 264, 129
Somov, B. V. 1992, Physical Processes in Solar Flares, Kluwer Academic Publ., Dordrecht
Somov, B. V. 2006, Solar System Res., 40, 85
Sterling, A. C., Moore, R. L., & Thompson, B. J. 2001, ApJ, 561, L219
Sturrock, P. A. 1966, Nature, 211, 695
Sturrock, P. A., Weber, M., Wheatland, M. S., & Wolfson, R. 2001, ApJ, 548, 492
Sui, L., Holman, G. D., & Dennis, B. R. 2006, ApJ, 646, 605
Sui, L., Holman, G. D., & Dennis, B. R. 2008, Adv. Space Res., 41, 976
Tousey, R., et al. 1973, Sol. Phys., 33, 265
Uralov, A. M. 1990, Sol. Phys., 127, 253
Uralov, A. M., Lesovoi, S. V., Zandanov, V. G., & Grechnev, V. V. 2002, Sol. Phys., 208, 69
White, S. M., Thomas, R. J., & Schwartz, R. A. 2005, Sol. Phys., 227, 231
Yokoyama T., & Shibata K. 1998, ApJL 494, 113
Yokoyama T., & Shibata K. 2001, ApJ 549, 1160